Post-print version:

Experimental Modelling and Optimal Torque Vectoring Control for 4WD Vehicles

E. Morera-Torres, C. Ocampo-Martinez, and F.D. Bianchi

This work has been published in **IEEE Transactions on Vehicular Technology**:

E. Morera-Torres, C. Ocampo-Martinez, and F.D. Bianchi, "Experimental Modelling and Optimal Torque Vectoring Control for 4WD Vehicles", *IEEE Transactions on Vehicular Technology*, vol. 71, nro. 20, pp. 4922-–4932, 2022.

Final version available at:

URL: https://ieeexplore.ieee.org/document/9732207

DOI: 10.1109/TVT.2022.3158091

BibTex:

```
@Article{Morera2022,
    Title   = {Experimental Modelling and Optimal Torque Vectoring Control for 4WD
       Vehicles},
    Author  = {Eduard Morera-Torres, Carlos Ocampo-Martinez, and Fernando D.
       Bianchi},
    Journal = {IEEE Transactions on Vehicular Technology},
    Year    = {2022},
    Number  = {20},
    Pages   = {4922-{4932},
    Volume  = {71},
    Doi     = {10.1109/TVT.2022.3158091}
}
```

Experimental Modelling and Optimal Torque Vectoring Control for 4WD Vehicles

Eduard Morera-Torres, Carlos Ocampo-Martinez *Senior Member, IEEE*, Fernando D. Bianchi

***Abstract*—This paper addresses the design of a torque vectoring architecture to control the four electrical machines in a four-wheel-drive (4WD) formula-type competition vehicle. The scheme includes a new yaw-rate controller and a novel optimal torque distribution algorithm. Two yaw-rate controllers are proposed: one based on $\mathcal{H}_\infty$ optimal control and another based on linear parameter varying (LPV) system concepts. Both controllers are designed using an extended bicycle model validated with experimental data. Simulation results shown the effectiveness of the proposed overall control scheme in terms of energy efficiency, cornering speed and stability no matter the high-demanding working conditions. Such an effectiveness is quantitatively demonstrated by means of several key performance indicators chosen to ease the comparison of the proposed approach with respect to other reported works.**

***Index Terms*—Torque vectoring, torque distribution, yaw-rate control, bicycle model, LPV modelling and control, $\mathcal{H}_\infty$ optimal control**

I. Introduction

In the last decade, the automotive industry has been increasingly committed to the electromobility together with a continuous desire of improving safety and comfort. These objectives have been reached in part by means of the implementation of modern control strategies in the vehicles, which allows to enhance vehicle stability and dynamic behaviour with, in some cases, better efficiency in terms of energy management. Most of those strategies are based on an optimal Torque Distribution (TD) among the vehicle actuators, a well-known control scheme called Torque Vectoring (TV). TV is used in both hybrid power-train vehicles [1], [2] and fully-electric power-train vehicles with either one or multiple actuators [3], [4], with the overall objective of improving energy management and efficiency [5] or maximizing the performance of a vehicle either off road or on a racing track. Most of these TV schemes rely on controlling the yaw moment around the vertical axis of the vehicle in order to suitably track a desired path using a yaw-rate control and a TD mechanism in a cascade configuration.

The benefits of using TV implementations in vehicles have been widely analyzed in the literature. For instance, in [6] an increase in the forces that the vehicle handles, together with a faster and better vehicle response is reported. The benefits in tracking performance achieved with the use of a TV scheme in in-wheel versus on-board motors is analyzed in [7]. Likewise, in [8] a slip angle control working together with the yaw-rate controller in order to adapt the vehicle limitations over multiple terrains is presented. Following the same line, in [9] the authors refer to the ability to include multiple driving modes. Benefits as the reduction of slip losses is demonstrated in [10]. All these works detail a general improvement in terms of stability and safety due to the TV implementation.

Regarding the yaw-rate controller, multiple alternatives have been proposed in the literature [11]. The proposals include schemes based on Proportional Integral Derivative (PID) strategies such as the ones in [12] or [13] focused on achieving a more stable behavior in a double-lane change maneuver. More advanced strategies based on sliding mode control are employed by Lacroix et al. [14] to improve stability compared to PID schemes. Linear quadratic control (LQR) have also been used to increase stability and path-tracking performance in [15], [16]. Robust control techniques such as $\mathcal{H}_\infty$ loop-shaping are utilized by Lu et al. [17] to achieve an increase in robustness and a better trade-off between control effort and performance when shaping the under-steering characteristic in quasi-static conditions without feed-forward. Adaptive strategies like the gain scheduled Linear Parameter-Varying (LPV) control presented in [18] have shown high stability and tracking performance. LPV controllers are based on gain-scheduling ideas in which the controller parameters are adapted to different operating conditions. This a popular technique to employ linear control tools in nonlinear systems.

Regarding the second module inside a TV algorithm, the TD problem, two approaches can be found. The first consists in applying equally accelerating-braking torques to generate the yaw moment [6]. The second implements the TD based on a direct relationship between wheel torques and the vertical tire forces [19]. This second study presents better results than the first one, but none of both focusing on energy management. More advanced schemes using energy-loss optimization are introduced in [20], [21]. Alcantar et al. [1] employ unconstrained optimization to produce the TD considering longitudinal forces throughout the slip ratio. Model Predictive Control (MPC) strategies based on constrained optimization are reported in [22], [23], [24]. Although these strategies are commonly integrated in autonomous vehicles, they are computational demanding and this might limit their use in high speed applications. In addition, racing drivers do not feel comfortable with this kind of strategies as they might limit the driver's ability to fully control the vehicle.

This paper proposes a new TV control system architecture

E. Morera-Torres and C. Ocampo-Martinez are with Automatic Control Department, Universitat Politècnica de Catalunya, Barcelona, Spain. e-mail: {eduard.morera,carlos.ocampo}@upc.edu

F.D. Bianchi is with the Instituto Tecnológico Buenos Aires (ITBA) and Consejo Nacional de Investigaciones Científicas y Técnicas (CONICET), Ciudad Autónoma de Buenos Aires, Argentina. e-mail: febianchi@itba.edu.ar

Manuscript received XXX, XX, 2015; revised XXX, XX, 2015.

for 4WD electric vehicles based on optimal control for the yaw-rate and constrained optimization to achieve the TD. The main contributions of this work are summarized as follows:

1) The statement and validation of a novel experimental-data-based control-oriented LPV model of the commonly used two-Degrees-of-Freedom bicycle model [25], extended to include transient regimes. The proposed model includes the understeering or oversteering vehicle behaviour in order to achieve more realistic predictions.
2) The design and comparison of two yaw-rate control strategies: one based on $\mathcal{H}_\infty$ optimal control and another on gain-scheduled LPV techniques. The design of both strategies relay on the proposed control-oriented LPV model.
3) A new TD algorithm based on multi-objective optimization, constrained by both longitudinal and lateral tire forces, following the idea of the unconstrained approach reported in [1]. In this new TD scheme, the optimization problem is fed with the tire information, the driver's commands and the signal produced by yaw-rate controller.

The remainder of the paper is organized as follows. In Section II, the overall proposed control scheme is presented. Section III introduces a two-Degrees-of-Freedom bicycle model based on experimental data that is latter used to design the yaw-rate controllers. The proposed TD algorithm is presented in Section IV. The complete control scheme is evaluated by extensive simulations using IPG-CarMaker in Section V. Finally, some concluding remarks are drawn in Section VI.

II. Proposed Control Scheme

The object of study in this paper is a vehicle prototype equipped with four independently driven electrical machines within the framework of the Formula Student (FS) competition[1]. Given the multiple actuators included in the powertrain, a control system is necessary to ensure a suitable coordination among these actuators, taking into account the driving intentions and the dynamical limitations of the vehicle.

The proposed control strategy is presented in Figure 1. The driver sets two target signals, a reference longitudinal force $F_{x,V}^{\mathrm{ref}}$, directly related to the pedal position, and the steering angle δ. This latter signal is then translated into a reference yaw moment $M_{z,TV}^{\mathrm{ref}}$ by the yaw-rate controller according to the steering angle δ, the measured yaw-rate $\dot{\psi}$ and the slip angle β. The yaw-rate control consists of an either LTI or LPV controller designed from a non-linear bicycle model based on experimental data as detailed in Section III. The target signals are used as set-points for the TD-related multi-objective optimization problem described and further discussed in Section IV. Such an optimization problem aims to produce a set of four torque commands (Γ_{FL}, Γ_{FR}, Γ_{RL}, and Γ_{RR}) for the four electric motors in order to maximize stability and performance in all working conditions.

It is crucial for the control algorithm to be constantly fed by real-time information. The sensors in the Inertial Navigation Systems (INS) and Inertial Measuring Units (IMU) on-board allow the measurements of velocities, accelerations and yaw-rate, while position sensors the capture of the driver steering and pedal commands. Tires information can also be calculated by using position sensors or, even better, estimators in order to complement and improve the INS data. In this case, the automotive software IPG-CarMaker[2] can be used to calculate all the above mentioned data.

III. Yaw-Rate Controller

A. Model Based on Experimental Data

The *two Degrees-of-Freedom Bicycle Model* in Figure 2 is widely used for control design purposes since it suitably approximates the steady-state cornering behaviour of a vehicle. However, multiple approaches have been presented and tested to improve the basic model in order to achieve a more accurate parametrization of the yaw dynamics [25]. Studies which show an improvement of this model focus on including the nonlinear behaviour of the tire. For instance, in [26] a piece-wise tire model is used to include the dependence of longitudinal force on slip ratio.

The aim of the extended model proposed in this paper is to overcome the limitations of the *two Degrees-of-Freedom Bicycle Model* with constant cornering stiffness coefficients that unavoidably affect the performance of the resulting control systems. In this case study, the lateral force dependence on slip angle is included through a parametrization of the cornering stiffness. The proposed model, from now on referred to as *extended bicycle model*, is given by the following equations:

$$\dot{\beta} = \frac{-(C_f(\beta)+C_r(\beta))}{m\,v}\beta - \left(1+\frac{C_f(\beta)\,l_f - C_r(\beta)\,l_r}{m\,v^2}\right)\dot{\psi} + \frac{C_f(\beta)}{m\,v}\,\delta, \tag{1a}$$

$$\ddot{\psi} = \frac{C_r(\beta)\,l_r - C_f(\beta)\,l_f}{J_v}\,\beta - \frac{C_r(\beta)\,l_r^2 + C_f(\beta)\,l_f^2}{J_v\,v}\,\dot{\psi} + \frac{C_f(\beta)\,l_f}{J_v}\,\delta + \frac{1}{J_v}\,M_{z,TV}, \tag{1b}$$

where m [kg] is the mass of the vehicle, J_v [kg m^2] is the inertia of the vehicle around the Z axis, δ [rad] is the steering angle of the front axle, l_f [m] is the distance between the CoG (Center-of-Gravity) and the front axle, l_r [m] is the distance between the CoG and the rear axle.

The non-linear phenomena associated to the tires, usually described with the Pacejka's formulation [27], is reflected both at the relation between lateral tire forces and its correspondent slip angle and at the cornering stiffness curve. This non-linearity is included in the model throughout a novel

[1]Formula Student is an engineering competition held annually worldwide where teams from universities around the world design, build, test, and race a small-scale formula style racing car. IMechE Official website: https://www.imeche.org/events/formula-student

[2]More information and further details about this software can be found at https://ipg-automotive.com

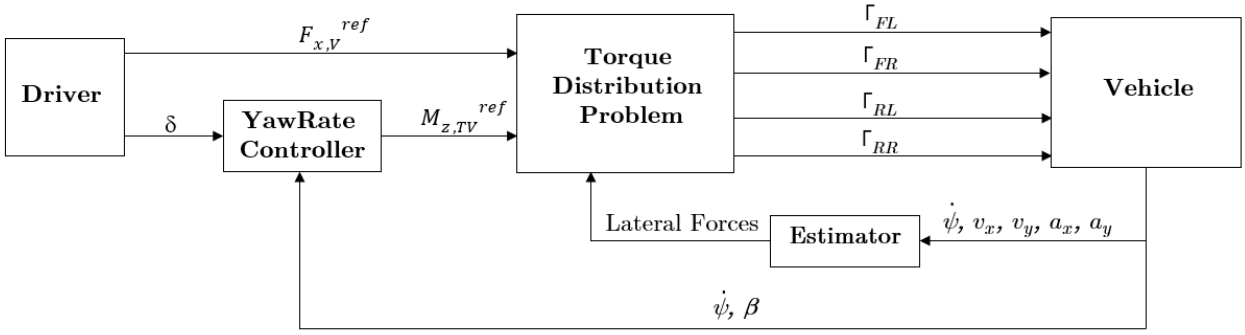

Fig. 1. Scheme of the proposed control strategy.

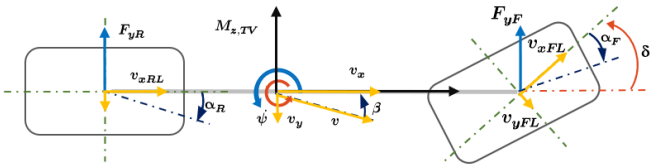

Fig. 2. Two Degrees-of-Freedom Bicycle Model.

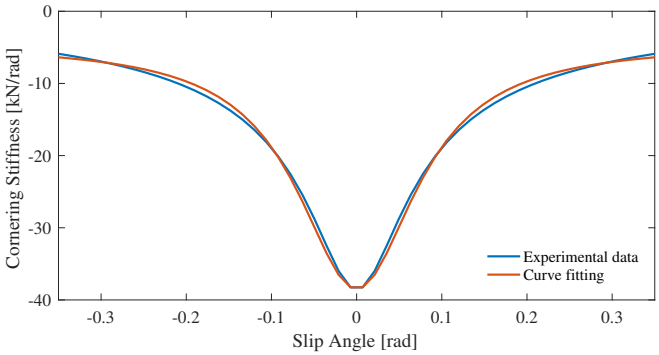

Fig. 3. Cornering Stiffness parametrization C_κ.

parametrization of the cornering stiffness coefficients obtained from experimental data. These coefficients are defined here as

$$C_\kappa(\beta) = \frac{\eta_\kappa \, \phi_\kappa}{\lambda_\kappa(\beta_\kappa) \, \beta^2 + \epsilon_\kappa}, \tag{2}$$

where C_κ [N/rad] refers to the cornering stiffness of the front ($\kappa = f$) or rear axle ($\kappa = r$). The parameter λ_κ allows the use of the cornering stiffness parametrization with the state variable β instead of the axle slip angle β_κ. The *experimental data* at Figure 3 comes from ($C_\kappa = F_{y,\kappa}/\beta_\kappa$), where $F_{y,\kappa}$ and β_κ have been experimentally obtained during tests on track. To obtain the parametrization in Figure 3, the parameters η_κ, ϕ_κ, λ_κ and ϵ_κ are determined by a curve fitting process, taking the presented *experimental data*. In this case, as both front and rear tires are the same, both axis coefficients result equal. In Figure 3, it can be seen that the data obtained with the proposed coefficient expression (2) properly fit the experimental data. The main advantage of using the approximation (2) is to have an expression that only depends on the slip angle β, an state in model (1).

The effect of the front and rear cornering stiffness coefficients can be assumed one depending on β and the other constant. Although the rear cornering stiffness is a dynamic phenomena [25], [27], even with this approximation the proposed model predicts a system behavior closer to the experimental data than previous models. This is shown in the next paragraphs.

Two tests have been carried out with the aim of validating the proposed model. The first test consists in driving the vehicle in an eight-shape circuit, also known as *skidpad*, in order to evaluate the yaw-rate developed in situations involving maximum lateral acceleration and fast turning direction change. Figure 4 shows a comparison between the experimental data logged during a test on tracks, the simulation data obtained using the nonlinear model (1) and the simulation data using a basic bicycle model [25], which is similar to (1) but with constant values for C_r and C_f. The relative error ϵ_{rel} between the experimental data and the response of both models is assessed as

$$\epsilon_{rel} = \frac{||s - s_m||_2}{||s||_2} \, 100\%, \tag{3}$$

where s and s_m are the simulated and measured signals, respectively. Then, the non-linear model response shows a fitting error of 13.7% compared to the real data, while the error fitting of the basic bicycle model is higher than 31%.

The second validation test was performed by comparing the response of the non-linear bicycle model with data logged when the vehicle was driven in an FS circuit. This test is particularly interesting as it covers a wide range of working conditions. The results are shown in Figure 5. The model (1) also exhibits a suitable estimation of the vehicle behavior.

B. Controller Design

The main objective of the yaw-rate controller is to ensure a suitable yaw-rate. For this purpose, two controllers are presented in this section: one based on $\mathcal{H}_\infty$ optimal control tools and another, with adaptive capabilities, using LPV techniques with the speed v and the slip angle β as scheduling variables. LPV controllers can be seen as optimal linear controllers with parameters that are modified in real-time according to a set of scheduling variables in order to

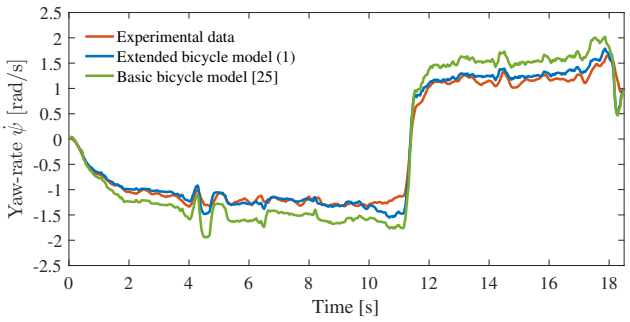

Fig. 4. Comparison between experimental and simulation responses when the vehicle is driven in a skidpad test circuit.

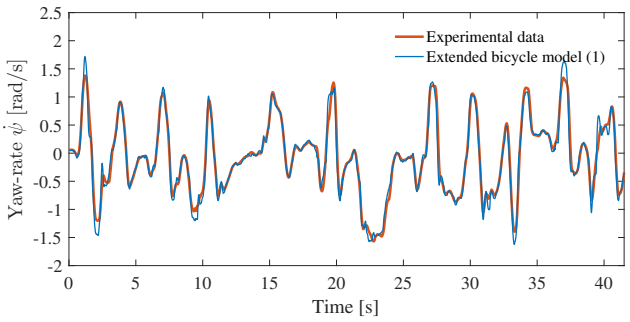

Fig. 5. Comparison between real and simulation responses when the vehicle is driven in a FS test circuit.

adapt itself to different operating conditions. The LPV control is a version of the popular gain-scheduling techniques with improvement in the design algorithm. The main appeal of gain-scheduling techniques is the possibility of extending the intuition of linear control design in nonlinear system.

$\mathcal{H}_\infty$ optimal control and LPV techniques seek a controller that solve the following optimization problem:

$$\min_{K\in\mathcal{K}} \frac{||z||_2}{||w||_2}, \tag{4}$$

where z is a performance signal, w the closed-loop input and $\|x\|_2 = \int_0^\infty x^T x\, dt$ the 2-norm of the signal x. In case of $\mathcal{H}_\infty$ optimal control, K is sought in the set of stabilizing LTI controllers $\mathcal{K}$. In case of LPV techniques, the set $\mathcal{K}$ consists of the stabilizing LPV controllers with scheduling variables v and β.

The yaw-rate control can be cast as illustrated in Figure 6. The objective is to track a yaw-rate reference $\dot{\psi}_{\text{ref}}$, whereas a bounded control action $M_{z,TV}$ and robustness are ensured. These objectives are stated by selecting

$$z = \begin{bmatrix}\tilde{e}\\ \tilde{u}\end{bmatrix} = \begin{bmatrix}W_e(s)(\dot{\psi}_{\text{ref}} - \dot{\psi}),\\ W_u(s)M_{z,TV}.\end{bmatrix}.$$

The weight W_e penalizes the tracking error at low frequencies. On the other hand, W_u penalizes the control action at high frequencies to guarantee a proper implementation and robustness against modelling errors. These weights are defined as

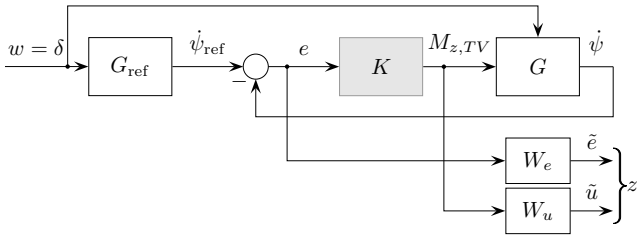

Fig. 6. Yaw-rate control design setup

$$W_e(s) = k_e \frac{s/10\omega_e + 1}{10s/\omega_e + 1}, \tag{5a}$$

$$W_u(s) = k_u \frac{10s/\omega_u + 1}{s/10\omega_u + 1}, \tag{5b}$$

where k_e, ω_e, k_u, and ω_u are design parameters.

The yaw-rate reference is set as

$$G_{\text{ref}} = \frac{v_0}{l(1 - K_u v_0^2)}, \tag{6}$$

where v_0 [m/s] is constant representative velocity of the CoG, l [m] is the wheelbase of the vehicle and K_u is the understeering coefficient. It is important to mention that the yaw rate reference signal is corrected in further simulations, if needed, through a weighing factor which depends on the side slip angle in order to ensure safe driving conditions. This methodology is detailed in [28].

Both controllers are designed with the same setup shown in Figure 6. In the case of the $\mathcal{H}_\infty$ controller, the plant G is an LTI model obtained from linearizing (1) at an operating point given by v_0 and β_0.

On the other hand, the design of the LPV controller is based on the nonlinear model (1), which is expressed as a quasi-LPV model

$$G: \begin{cases} \dot{x} = A(\beta, v)x + B_1(\beta, v)\delta + B_2 M_{z,TV}, \\ y = Cx, \end{cases} \tag{7}$$

where the state vector is $x = [\beta\ \dot{\psi}]^T$,

$$\begin{bmatrix}A(\beta,v) & B_1(\beta,v)\end{bmatrix} = \begin{bmatrix}A_0 & B_{1,0}\end{bmatrix} + \sum_{i=1}^{5} f_i(\beta, v)\begin{bmatrix}A_i & B_{1,i}\end{bmatrix},$$

$B_2 = [0\ 1/J_v]^T$, and $C = [0\ 1]$. Functions $f_i(\cdot)$ are defined as

$$f_1(\beta) = C_f(\beta), \qquad f_2(\beta, v) = C_f(\beta)/v,$$
$$f_3(v) = 1/v, \qquad f_4(\beta, v) = C_f(\beta)/v^2,$$
$$f_5(v) = 1/v^2,$$

and the constant matrices A_i and B_i $(i = 0, \ldots, 5)$ are selected such that both the extended model (1) and the LPV model (7) represent the same differential equations. Notice that C_r is assumed constant as mentioned in Section III-A.

Model (7) can be used to design an LPV controller by using tools such as those in [29]. However, such design would

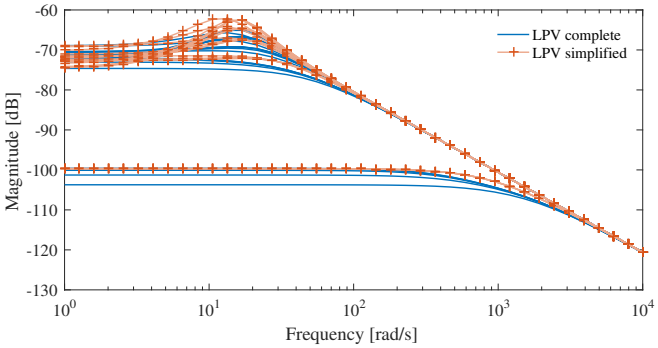

Fig. 7. Frequency responses corresponding to LTI obtained at frozen parameter values of the complete and simplified LPV model

result in a controller rather complex to implement. A trade-off can be reached considering part of the nonlinear terms in (7) as additive uncertainty. In particular, the model (7) can be simplified as

$$G_r : \begin{cases} \dot{x} = A(\rho_1, \rho_2)x + B_1(\rho_1, \rho_2)\delta + B_2 M_{z,TV}, \\ y = Cx, \end{cases} \tag{8}$$

where

$$\begin{bmatrix} A(\rho_1,\rho_2) & B_1(\rho_1,\rho_2) \end{bmatrix} = \begin{bmatrix} A_0 & B_{1,0} \end{bmatrix} + \rho_1 \begin{bmatrix} A_1 & B_{1,1} \end{bmatrix} + \rho_2 \begin{bmatrix} A_3 & B_{1,3} \end{bmatrix},$$

$\rho_1 = C_f(\beta)$, and $\rho_2 = 1/v$. Figure 7 shows the frequency responses corresponding to frozen parameter values for the complete model in (7). The differences between the complete quasi-LPV model (7) and the approximated one (8) are quite small and can be taken into account in the controller design with a proper selection of the parameters of W_u.

The resulting LPV controller is given by

$$K(\rho) : \begin{cases} \dot{x}_c = A_c(\rho)x_c + B_c(\rho)e, \\ u = C_c(\rho)x_c + D_c(\rho)e, \end{cases}$$

where x_c is the controller state vector, and

$$\begin{bmatrix} A_c(\rho) & B_c(\rho) \\ C_c(\rho) & D_c(\rho) \end{bmatrix} = \begin{bmatrix} A_{c,0} & B_{c,0} \\ C_{c,0} & D_{c,0} \end{bmatrix} + \sum_{i=1}^{2} \rho_i \begin{bmatrix} A_{c,i} & B_{c,i} \\ C_{c,i} & D_{c,i} \end{bmatrix}.$$

with $A_{c,i}$, $B_{c,i}$, $C_{c,i}$ and $D_{c,i}$ constant matrices produced with the design algorithm in order to solve the optimization problem (4). Notice that the implementation of the LPV controller is similar to any LTI one once the previous matrices are updated with the measures of v and β.

IV. Torque Distribution

As presented in Figure 1, there are two control signals, $F_{x,V}^{ref}$ and $M_{z,TV}^{ref}$, determined by the driver, that should be tracked by a coordinated action between the four vehicle actuators. With this tracking objective, a constrained TD-related multi-objective optimization problem (Section IV-C) is designed with the aim to establish the best possible (optimal) combination of wheel torques that ends up generating a suitable $F_{x,V}$ and $M_{z,TV}$ based on a quasi-static vehicle model (Section IV-A). In the case study considered in this paper, the TD optimization problem must converge to an optimal solution within the period of T_s=20 ms, which is the established sampling time determined by the electrical machines controllers.

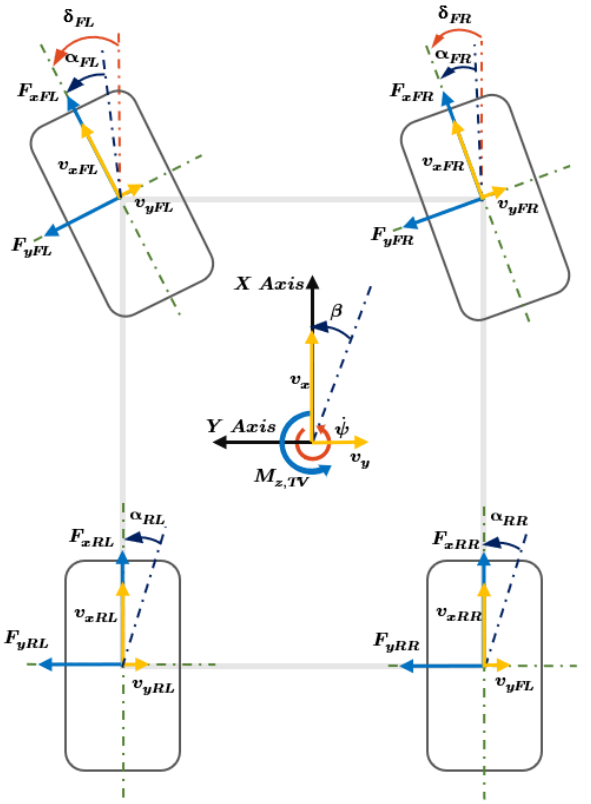

Fig. 8. Vehicle Free-Body Diagram illustrating the forces applied to the vehicle

A. Quasi-Static Model

The free-body diagram[3] shown in Figure 8 illustrates the forces applied to the vehicle through the tires. The corresponding expressions in terms of the wheel torque vector $\mathbf{\Gamma} = [\Gamma_{\mathrm{FL}}\ \Gamma_{\mathrm{FR}}\ \Gamma_{\mathrm{RL}}\ \Gamma_{\mathrm{RR}}]^T$ are

$$F_{x,V}(\mathbf{\Gamma}) = \frac{1}{R_w}\begin{bmatrix} \cos(\delta_1) & \cos(\delta_2) & 1 & 1 \end{bmatrix}\mathbf{\Gamma}, \tag{9a}$$

$$M_{z,TV}(\mathbf{\Gamma}) = \frac{1}{R_w}\begin{bmatrix} -\Lambda(\delta_1) & \Lambda(\delta_2) & -\frac{t_f}{2} & \frac{t_f}{2} \end{bmatrix}\mathbf{\Gamma}, \tag{9b}$$

with $\Lambda(\delta_i) = l_f \sin(\delta_i) - \frac{t_f}{2}\cos(\delta_i)$, where δ_i [rad] $(i = 1, 2)$ is the steering angle for each of the front tires, t_f [m] is the front track, t_r [m] is the rear track and R_ω [m] is the wheel radius. Expressions in (9) are used to solve the TD-related optimization problem determining the individual set-point torques for each one of the electrical machines.

[3]Please note that that the self-aligning torques of the tires [30] are not considered due to their low values compared to the yaw moment generated by the tire forces in order to simplify (9).

B. Friction circle of the tires

The friction circle of a tire has been widely studied in the literature, see e.g. [31], [30]. In this paper, a simplified version defined by longitudinal ($F_{x,i}$) and lateral forces ($F_{y,i}$) is considered in order to introduce the dynamic limitations in terms of grip inside the TD ($i \in \{\mathrm{FL}, \mathrm{FR}, \mathrm{RL}, \mathrm{RR}\}$).

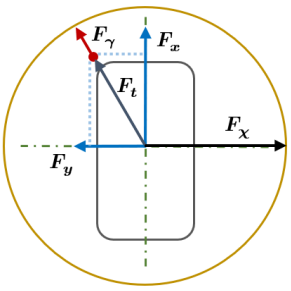

Fig. 9. Simplified friction circle of a tire

For a tire $i \in \{\mathrm{FL}, \mathrm{FR}, \mathrm{RL}, \mathrm{RR}\}$, expression (10) governs the working point inside a simplified circle of friction, $F_{wp,i}\,(F_{x,i}(\sigma_i, F_{z,i}), F_{y,i}(\beta_i, F_{z,i}))$ and σ_i is the slip ratio of the tire. To avoid exceeding the forces that a tire i is able to handle, $F_{wp,i}$ should always remain inside the limits of that circle. Moreover,

$$F_{t,i} = \sqrt{{F_{x,i}}^2 + {F_{y,i}}^2}, \tag{10a}$$

$$F_{\chi,i} = \mu\, F_{z,i}, \tag{10b}$$

$$F_{\gamma,i} = F_{\chi,i} - F_{t,i}, \tag{10c}$$

where $F_{x,i}$ corresponds to the longitudinal force, $F_{y,i}$ corresponds to the lateral force, $F_{t,i}$ [N] is the module of the force developed by the tire, $F_{\chi,i}$ [N] is the maximum force that the tire can support in certain conditions and $F_{\gamma,i}$ [N] is the extra force that the tire may support in a given instant.

Regarding the tire forces involved in the TD problem, multiple methodologies can be used to be obtained. In this study, both $F_{x,i}$ and $F_{y,i}$ are determined by using the Pacejka parametrization [27], in which case variables such as σ_i, α_i and $F_{z,i}$ are required. Another common methodology is by using estimators such as an Extended Kalman Filter (EKF), among others. The design of this estimators is out of the scope of this article, but detailed information regarding this topic can be found in [32], [33], [34].

C. Multi-Objective Optimization Problem

As shown in Figure 1, the yaw moment reference $M_{z,TV}^{\mathrm{ref}}$ and the longitudinal force reference $F_{x,V}^{\mathrm{ref}}$ are inputs for the TD multi-objective optimization problem. This optimization problem aims to fulfill the driver's acceleration and maneuver commands while considering the vehicle limitations, which take into account the tire and power limits. Such a multi-objective optimization problem is stated as follows:

$$\underset{\mathbf{\Gamma}}{\text{minimize}} \quad \sum_{m=1}^{3} \alpha_m J_m \tag{11a}$$

subject to

$$\Gamma_{i,\min} \leq \Gamma_i \leq \Gamma_{i,\max},, \tag{11b}$$

$$F_{x,V,\min} \leq F_{x,V}(\mathbf{\Gamma}) \leq F_{x,V,\max}, \tag{11c}$$

$$M_{z,TV,\min} \leq M_{z,TV}(\mathbf{\Gamma}) \leq M_{z,TV,\max}, \tag{11d}$$

$$\sum_{j=1}^{4} \frac{\Gamma_j\, \omega_j}{\eta_j} \leq P_{\max}, \tag{11e}$$

where $i \in \{\mathrm{FL}, \mathrm{FR}, \mathrm{RL}, \mathrm{RR}\}$, α_m $(m = 1, 2, 3)$ are prioritization factors, $F_{x,V}$ and $M_{z,TV}$ are the longitudinal force and the yaw moment given by (9a) and (9b), respectively. The limits $F_{x,V,\min}$, $F_{x,V,\max}$, $M_{z,TV,\min}$, and $M_{z,TV,\max}$ are imposed by the friction circle of the tires given by (9). The parameter η_j is the electro-mechanic efficiency corresponding to each electrical machine, ω_j [rad/s] is the angular velocity of each wheel and $P_{\max}$ [W] is the maximum allowable power.

The objective function (11a) consists of three terms that are next explained. The first term in (11a) (for $m = 1$) aims to minimize the error between the desired longitudinal force and the one developed by the vehicle, i.e.,

$$J_1 = \|F_{x,V} - F_{x,V}^{\mathrm{ref}}\|^2, \tag{12}$$

where $F_{x,V}^{\mathrm{ref}}$ [N], is the longitudinal force indicated by the driver. Although (12) is not considered the most important objective, it must be taken into account to considerably improve the driving experience when accelerating.

The second term in (11a) (for $m = 2$) minimizes the yaw-rate tracking error, i.e.,

$$J_2 = \|M_{z,TV} - M_{z,TV}^{\mathrm{ref}}\|^2. \tag{13}$$

As the main objective of a TV system is to improve the behaviour while cornering, this term is crucial to enhance the overall vehicle performance in terms of time-lap reduction.

The last term in the objective function (11a) (for $m = 3$) is written as

$$J_3 = \alpha_3 \sum_i \theta_i \Gamma_i^2, \tag{14}$$

with $i = \{\mathrm{FL}, \mathrm{FR}, \mathrm{RL}, \mathrm{RR}\}$, where θ_i are scalar weights. The implementation of this term seeks to achieve a suitable control over TD among each axle (or each electrical machine, if desired) that is going to be developed to reach the first two objectives. This control consideration results quite useful in offering the driver a versatile behaviour by implementing a more-likely or less-likely rear wheel power-train actuation, while also allows to proper manage the electrical machines temperatures.

V. Simulation Results

A. Control design settings

As mentioned in Section III-B, two yaw-rate controllers were designed using the weighting functions in (5) considering the following parameters:

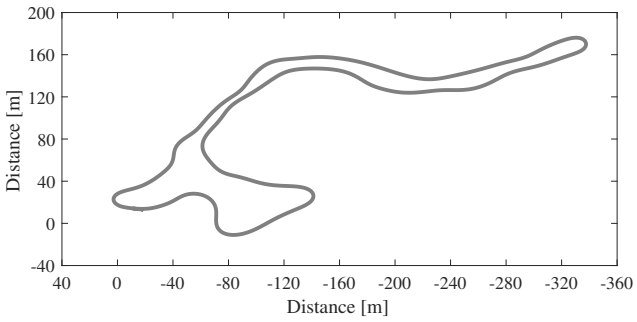

Fig. 10. Coordinates of the FS test circuit used in simulations.

- $\mathcal{H}_\infty$ controller: $k_e = 1$, $\omega_e = 0.1$ rad/s, $k_u = 0.05$, and $\omega_u = 10$ rad/s.
- LPV controller: $k_e = 0.1$, $\omega_e = 0.1$ rad/s, $k_u = 0.005$, and $\omega_u = 25$ rad/s.

The parameters of the LPV controller were assumed ranging in $14574 \leq \rho_1 \leq 28725$ and $0.03 \leq \rho_2 \leq 3.6$, which corresponds to $0 \leq \beta \leq 10$ degrees and $1 \leq v \leq 120$ km/h. In order to design the $\mathcal{H}_\infty$ controller, the nonlinear model was linearized at an operating point corresponding to $v_0 = 67$ km/h, $\delta_0 = 0.005$ rad and $M_{z,TV,0} = 0$ Nm. The K_u value to compute the reference signal was set at -0.003.

In order to evaluate the proposed TV control scheme, the closed-loop system was simulated with IPG-CarMaker for use with MATLAB/Simulink, a standard software used to validate these systems. A thorough parametrization of the vehicle has been carried in order to properly model a real FS competition vehicle. The test circuit used in all cases, except for the one presented in Section V-D, corresponds to a real FS test circuit shown in Figure 10. The aim of this test circuit is to reproduce a large range of driving situations, from sharp low-speed curves to open high-speed curves. Regarding the TD algorithm, the Quadratic Programming (QP) problem in (11) was solved at each sampling time using CPLEX[4] solver. The prioritization weights in the objective function (11) were set as $\alpha_1 = 0.2$, $\alpha_2 = 0.6$ and $\alpha_3 = 0.2$. This corresponds to Case 6 in Table II; a detailed analysis about the selection of these weights is given in Section V-B.

B. FS test circuit

Both yaw-rate controllers proposed in Section III-B were evaluated by simulation in case of the FS test circuit shown in Figure 10. The yaw-rate $\dot{\psi}$ and the corresponding references $\dot{\psi}^{\text{ref}}$ for both controllers are shown in the top and middle plots in Figure 11. The references in both cases results of applying (6) to the steering angle δ imposed by the driver. The yaw-rate $\dot{\psi}$ is consequence of the tire forces for both lateral and longitudinal forces (the ones controlled by the TV system).

[4]More information about the CPLEX solver: https://www.ibm.com/support/knowledgecenter/SSSA5P_12.9.0/ilog.odms.cplex.help/CPLEX. Other options could be CasADi: https://web.casadi.org or Gurobi: https://www.gurobi.com.

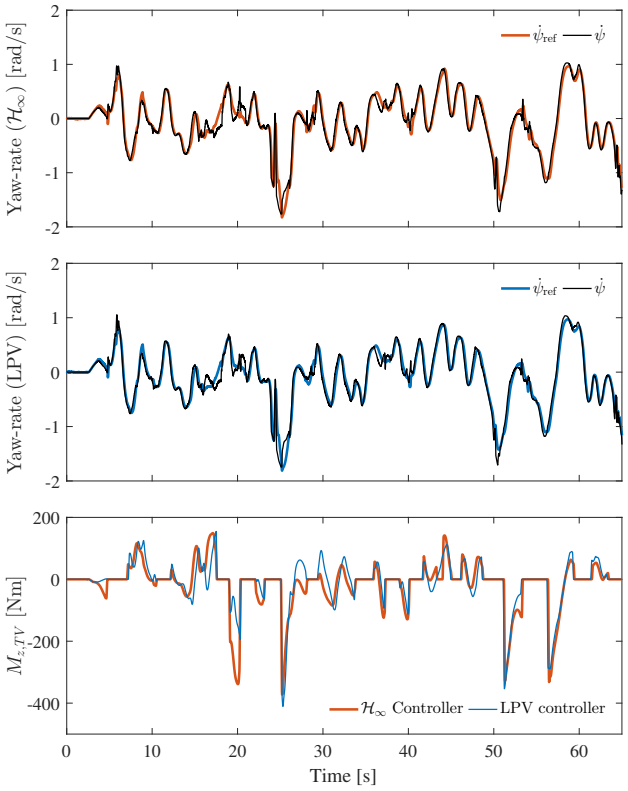

Fig. 11. Comparison between $\mathcal{H}_\infty$ and LPV controllers corresponding to closed-loop simulation for the FS test circuit in Figure 10.

The yaw-moment $M_{z,TV}$ generated by the the two yaw-rate controllers are presented in the bottom plot.

It can be observed that both controllers achieved a suitable reference tracking. However, the LPV controller demands slightly lower control action $M_{z,TV}$. The differences can be better quantified defining two key performance indicators (KPIs). In this case, the selected KPIs are the root square value of the tracking error (RMSE) and the integral of the absolute value of the control action (IACA). The former is an indicator of the quality in the yaw-rate reference tracking, while the latter evaluates the control effort needed to reach the desired tracking. The results obtained with each controller are summarized in Table I. From these KPIs, it can be concluded that the LPV controller achieved a slightly better reference tracking with considerable lower control effort. The implementation of the LPV controller requires two additional measurements (the scheduling variables v and β), which can be obtained from the available INS sensor, and updating the controller matrix functions. Nevertheless, this is not a significant increase in the controller implementation complexity and the improvement that the LPV controller offers compared to the $\mathcal{H}_\infty$ one is enough to consider it as the most suitable option to be implemented and tested. In the following tests, only the LPV based yaw-rate control will be used.

Figure 12 shows the yaw-moment, the force, the torque developed by each motor and the power corresponding to the

TABLE I
KPI COMPARISON BETWEEN $\mathcal{H}_\infty$ AND LPV CONTROLLERS

Controller	RMSE ($\dot{\psi}$) [rad/s]	IACA ($M_{z,TV}$) [Nm]
$\mathcal{H}_\infty$	0.8662	2186.4
LPV	0.8628	2042.7

closed-loop system with the LPV controller. The yaw-moment reference $M_{z,TV}^{\text{ref}}$ produced by the yaw-rate controller and the one actually applied by the TD algorithm can be seen in the top plot. The TD algorithm is able to distribute the torque among the four wheels while the total yaw-moment $M_{z,TV}$ is close to the one demanded by the yaw-rate controller. In plot c), it can be seen the reference and the developed $F_{x,V}$. By implementing Case 6 of the TD problem, the $F_{x,V}$ error minimization has lower priority compared with the $M_{z,TV}$ one. The main reason of the larger difference between the reference and developed $F_{x,V}$ in comparison to the $M_{z,TV}$ is not due to the $F_{x,V}$ lower priority, but because of the power limitation and the tire saturation constrains. This can be concluded from the plots c) and d) in Figure 12. When The power limitation takes action, the tracking error of $F_{x,V}$ increases. Nevertheless, the tracking of $F_{x,V}^{\text{ref}}$ can be considered satisfactory for a practical point of view.

The torques developed by each wheel can be seen in Figure 12c). These are the outputs of the TD-related optimization problem. Some interesting conclusions can be drawn from this plot. First, it is clear that during a whole lap, torques developed by the rear motors are larger than those torques developed by the front ones[5] as a consequence of the TD problem parametrization with the objective of enhancing a more similar rear-wheel drive behavior. This suitable power distribution also leads to a coordinated actuation of the motors in which none of them work excessively over nominal conditions, which allow to have better control over the motors temperature and, as a consequence, energy efficiency is enhanced.

Finally, in the bottom plot in Figure 12, the suitable implementation of the power limitation inside the TD can be observed. In order not to exceed the power rate of the electric equip, the limitations might be slightly below the maximum allowed value. Due to the sampling time in which the calculations are done, a little overshoot could appear, reason why the maximum limit should be set around 78 kW.

C. TD comparison

As previously mentioned in Section IV-C, the TD-related optimization problem involves three objectives. In order to analyze the most adequate prioritization for each of them, multiple lap simulations have been performed to compare such objectives and to decide the most convenient combination of weights (optimization-based control tuning) based on two new KPIs. These indicators are the *Lap Time* and the *Energy Consumption* during one lap (Table II), and the results corresponding to Case 6 are reported in Figure 12.

[5]Please notice that this comparison must be based on analyzing right and left side electrical machines independently, not to consider the generated $M_{z,TV}$ as a variable in this sub-analysis.

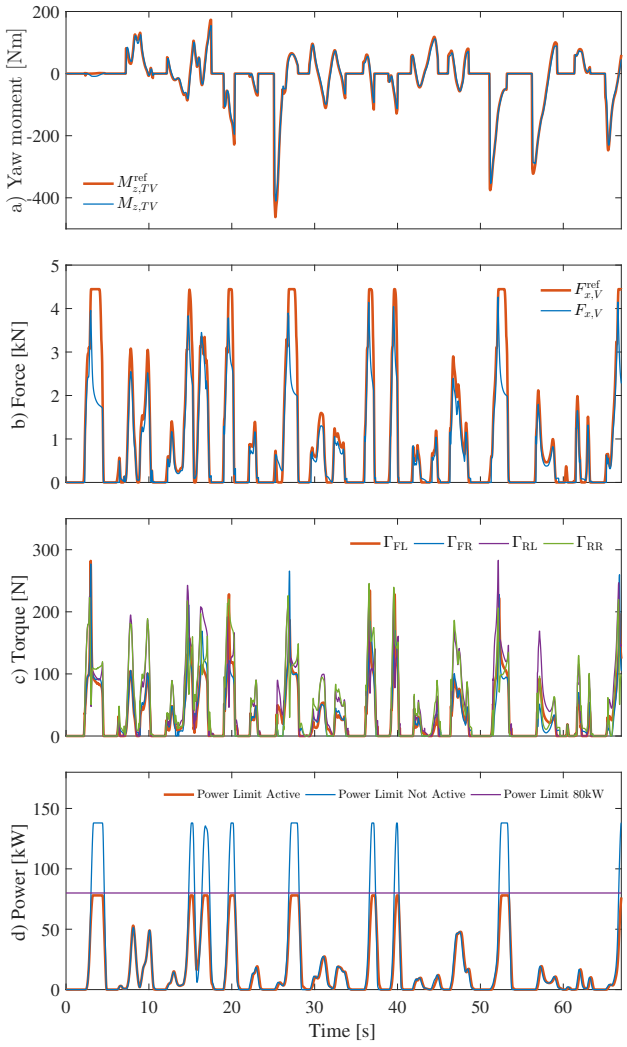

Fig. 12. Simulation results using the LPV yaw-rate controller in case of the FS test circuit in Figure 10.

TABLE II
KPI OBTAINED WITH SEVERAL PRIORITY WEIGHTS IN THE OPTIMIZATION PROBLEM (11).

Case	Objectives Weights [%]			Lap Time [s]	Energy [Wh]
	α_1	α_2	α_3		
1	40	50	10	59.06	267.31
2	30	60		59.08	272.32
3	20	70		58.55	280.32
4	10	80		58.95	272.05
5	30	50	20	58.65	268.65
6	20	60		58.28	276.37
7	10	70		58.94	266.71

From Table II, some interesting conclusions can be drawn. Referring to the Lap Time KPI, it can be seen that neither prioritizing the $M_{z,TV}$ nor the $F_{x,V}$ significantly improve the results, but around a 65-25% ratio seems to be the most convenient option in terms of reducing such a KPI. Also from this analysis, it can be determined that, although not being the best option, maximizing the $M_{z,TV}$ would be better that doing so with $F_{x,V}$.

Besides, referring to energy consumption, directly related to control effort, a reduction of about 5% is achieved between cases. This is an important consideration since a reduction in energy consumption leads to a larger distance range or, quite important in racing, lowering battery dimensions leading to weight reduction.

Finally, the J_3 term of (11) and its prioritization weight are discussed. J_3 is considered as the component of the TD function which allows to manage the power proportion to each axle that determines how the other two objectives are achieved. At first sight, it could be said that neither giving more nor less priority to J_3 affects energy consumption of the vehicle in a significant way. However, analyzing at the same time both KPIs, it is remarkable that, with the same amount of energy, Lap Time gets reduced with a larger α_3.

Once the considered possibilities to tune the TD-related multi-objective optimization problem are presented (Table II), it can be concluded that the most suitable configuration corresponds to Case 6.

D. Active vs. not-active TV comparison

In order to evaluate the benefits of using the proposed TV, the closed-loop model with the LPV controller is compared with the case in which TV is not active, i.e. the torque is equally distributed $\Gamma_{\mathrm{FL}} = \Gamma_{\mathrm{FR}} = \Gamma_{\mathrm{RL}} = \Gamma_{\mathrm{RR}} = 0.25\Gamma_{\mathrm{tot}}$ (the total torque). In this case, simulations were carried out in the skidpad test circuit shown in the top plot in Table Figure 13. The reason to present this kind of results is due to the fact that it allows us to study transient conditions at the entry of a lap and at the driving direction change between laps 2 and 3, together with steady-state conditions through each lap. A part from that, it is a standardized test and it allows to suitably evaluate results such as the ones in III. Similar results have been obtained in a slalom test, so it has not been included to avoid redundancy.

In this test, the vehicle should complete two laps turning left (Laps 1 & 2), change cornering direction, and other two laps turning right (Laps 3 & 4). The lower plots in Figure 13 shows the yaw-rate $\dot{\psi}$ and its corresponding reference. In both cases, the aim is to reach the maximum average $\dot{\psi}$ in order to reduce the lap time[6]. It can be observed that when the TV is active, the vehicle takes less time to finish the test, as the TV system improves the average achieved yaw-rate and corrects the natural understeering behaviour of the vehicle, leading to higher cornering speed.

Table III summarizes different characteristics observed in the yaw-rate responses shown in Figure 13. When the TV

[6]In a skidpad test, the measured time for each turning direction corresponds to the second lap for each direction (which are laps 2 & 4).

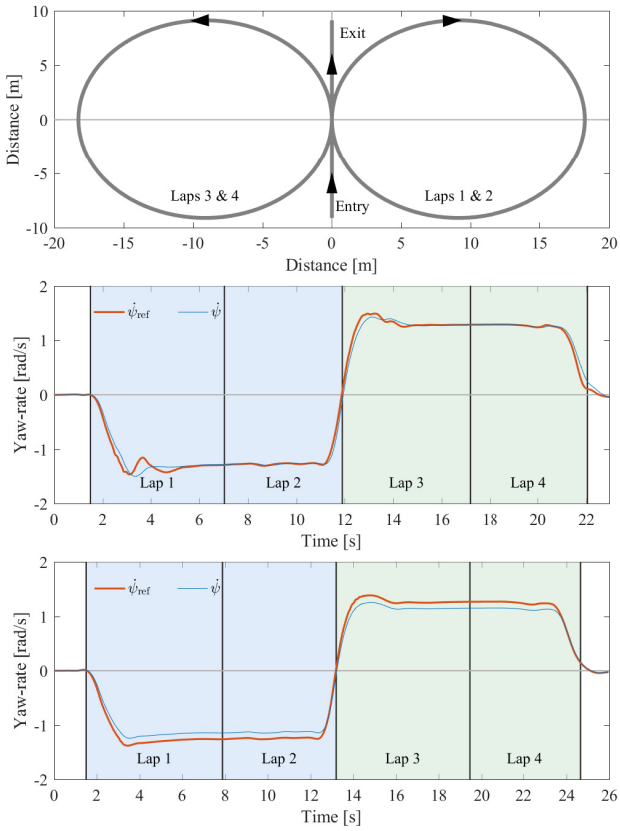

Fig. 13. Yaw-rate tracking comparison between the proposed TD scheme and the used of equally torque distribution. Top: skidpad test circuit, middle: response with the proposed TD scheme, bottom: response with torque equally distributed

TABLE III
DIFFERENT CHARACTERISTICS OBSERVED IN THE YAW-RATE RESPONSES IN FIGURE 13

Characteristic	TV enabled	TV disabled	Units
Peak yaw-rate	1.5	1.26	rad/s
Average yaw-rate (during laps)	1.29	1.18	rad/s
Lap 2 duration	4.87	5.32	s
Lap 4 duration	4.85	5.20	s
Average duration	4.86	5.26	s

is active, the general cornering performance of the vehicle improves quite considerably. The average yaw-rate increases 0.11 rad/s when the TV is active, 9.3% increase in comparison with the response when TV is not active. This improvement allows the vehicle to reduce the skidpad time in 0.4 s, which is quite noticeable considering that when TV not active this time increases to 5.26 s.

VI. CONCLUDING REMARKS

This paper has proposed a new closed-loop control scheme for the efficient TD among the four electrical machines in 4WD formula-type competition vehicles. The proposed scheme consists of a yaw-rate control and an optimization based algorithm to distributed the torque among the wheels. Two control strategies, an $\mathcal{H}_\infty$ and an LPV control approach, have been considered and compared for the design of the yaw-

rate controller. Both controllers were designed using a novel and improved version of the well-known bicycle model, which has been validated with experimental data.

The solution of the constrained TD-related multi-objective optimization problem has shown to suitably distribute the power among the four electrical machines while fulfilling the yaw-rate controller and longitudinal force demands. In general terms, the TV implementation has shown a quite noticeable improvement in achievable yaw-rate, cornering speed, stability and ability to constantly work over high-demanding working conditions. Moreover, results have also shown the enhancement in energy efficiency given the versatility offered in terms of vehicle behavior.

As further work, the inclusion of regenerative braking inside the TV algorithm will be considered together with the use of an improved tire model to achieve better results and tire forces control together with tire waste management.

REFERENCES

[1] J. V. Alcantar and F. Assadian, "Vehicle dynamics control of an electric-all-wheel-drive hybrid electric vehicle using tyre force optimisation and allocation," *Vehicle System Dynamics*, vol. 57, no. 12, pp. 1897–1923, 2019.

[2] M. Sivertsson, C. Sundström, and L. Eriksson, "Adaptive control of a hybrid powertrain with map-based ECMS," in *Proc. of the 18th IFAC World Congress*, vol. 44, no. 1, 2011, pp. 2949–2954.

[3] G. Park, K. Han, K. Nam, H. Kim, and S. B. Choi, "Torque vectoring algorithm of electronic-four-wheel drive vehicles for enhancement of cornering performance," *IEEE Transactions on Vehicular Technology*, vol. 69, no. 4, pp. 3668–3679, 2020.

[4] L. Zhai, T. Sun, and J. Wang, "Electronic stability control based on motor driving and braking torque distribution for a four in-wheel motor drive electric vehicle," *IEEE Transactions on Vehicular Technology*, vol. 65, no. 6, pp. 4726–4739, 2016.

[5] A. Parra, D. Tavernini, P. Gruber, A. Sorniotti, A. Zubizarreta, and J. Pérez, "On nonlinear model predictive control for energy-efficient torque-vectoring," *IEEE Transactions on Vehicular Technology*, vol. 70, no. 1, pp. 173–188, 2021.

[6] J. Ghosh, A. Tonoli, and N. Amati, "A torque vectoring strategy for improving the performance of a rear wheel drive electric vehicle," in *Proc. of the IEEE Vehicle Power and Propulsion Conference (VPPC)*, 2015, pp. 1–6.

[7] T. Goggia, A. Sorniotti, L. D. Novellis, A. Ferrara, P. Gruber, J. Theunissen, D. Steenbeke, B. Knauder, and J. Zehetner, "Integral sliding mode for the torque-vectoring control of fully electric vehicles: theoretical design and experimental assessment," *IEEE Transactions on Vehicular Technology*, vol. 64, no. 5, pp. 1701–1715, 2015.

[8] B. Lenzo, M. Zanchetta, A. Sorniotti, P. Gruber, and W. D. Nijs, "Yaw rate and sideslip angle control through single input single output direct yaw moment control," *IEEE Transactions on Control Systems Technology*, vol. 29, no. 1, pp. 124–139, 2021.

[9] L. De Novellis, A. Sorniotti, P. Gruber, J. Orus, J.-M. R. Fortun, J. Theunissen, and J. De Smet, "Direct yaw moment control actuated through electric drivetrains and friction brakes: Theoretical design and experimental assessment," *Mechatronics*, vol. 26, pp. 1–15, 2015.

[10] V. Ivanov, K. Augsburg, and D. Savitski, "Torque vectoring for improving the mobility of all-terrain electric vehicles," in *Proc. of the 12th European Regional Conference of the International Society for Terrain-Vehicle Systems*, 2012.

[11] A. Medina, G. Bistué, and A. Rubio, "Comparison of typical controllers for direct yaw moment control applied on an electric race car," *Vehicles*, vol. 3, pp. 127–144, 2021.

[12] L. Shao, A. Karci, D. Tavernini, A. Sorniotti, and M. Cheng, "Design approaches and control strategies for energy-efficient electric machines for electric vehicles - a review," *IEEE Access*, vol. 8, pp. 116 900–116 913, 2020.

[13] Z. Zainal, W. Rahiman, and N. R. Baharom, "Yaw rate and sideslip control using PID controller for double lane changing," *Journal of Telecommunication, Electronic and Computer Engineering*, vol. 9, pp. 99–103, 8 2017.

[14] B. Lacroix, Z. Liu, and P. Seers, "A comparison of two control methods for vehicle stability control by direct yaw moment," *Applied Mechanics and Materials*, vol. 120, pp. 203–217, 2012.

[15] N. Tavan, M. Tavan, and R. Hosseini, "An optimal integrated longitudinal and lateral dynamic controller development for vehicle path tracking," *Latin American Journal of Solids and Structures*, vol. 12, pp. 1006–1023, 2015.

[16] K. Miyahara, H. Fujimoto, Y. Hori, and V. Ivanov, "Performance benchmark of yaw rate controllers by active front steering: comparative analysis of model predictive control, linear quadratic integral control and yaw moment observer," in *Proc. of 45th Annual Conference of the IEEE Industrial Electronics Society (IECON)*, 10 2019, pp. 473–478.

[17] Q. Lu, A. Sorniotti, P. Gruber, J. Theunissen, and J. De Smet, "H_∞ loop shaping for the torque-vectoring control of electric vehicles: Theoretical design and experimental assessment," *Mechatronics*, vol. 35, pp. 32–43, 2016.

[18] G. Kaiser, Q. Liu, C. Hoffmann, M. Korte, and H. Werner, "Torque vectoring for an electric vehicle using an LPV drive controller and a torque and slip limiter," in *Proc. of the 51st IEEE Conference on Decision and Control (CDC)*, 2012, pp. 5016–5021.

[19] A. Parra, A. Zubizarreta, J. Pérez, and M. Dendaluce, "Intelligent torque vectoring approach for electric vehicles with per-wheel motors," *Complexity*, p. Article ID 7030184, 2018.

[20] L. D. Novellis, A. Sorniotti, and P. Gruber, "Wheel torque distribution criteria for electric vehicles with torque-vectoring differentials," *IEEE Transactions on Vehicular Technology*, vol. 63, no. 4, pp. 1593–1602, 2014.

[21] C. Chatzikomis, M. Zanchetta, P. Gruber, A. Sorniotti, B. Modic, T. Motaln, L. Blagotinsek, and G. Gotovac, "An energy-efficient torque-vectoring algorithm for electric vehicles with multiple motors," *Mechanical Systems and Signal Processing*, vol. 128, pp. 655–673, 2019.

[22] M. Schwartz, F. Siebenrock, and S. Hohmann, "Model predictive control allocation of an over-actuated electric vehicle with single wheel actuators," in *Proc. of the 10th IFAC Symposium on Intelligent Autonomous Vehicles (IAV)*, vol. 52, no. 8, 2019, pp. 162–169.

[23] Y. Ren, L. Zheng, and A. Khajepour, "Integrated model predictive and torque vectoring control for path tracking of 4-wheel-driven autonomous vehicles," *IET Intelligent Transport Systems*, vol. 13, no. 1, pp. 98–107, 2019.

[24] H. Peng, W. Wang, Q. An, C. Xiang, and L. Li, "Path tracking and direct yaw moment coordinated control based on robust MPC with the finite time horizon for autonomous independent-drive vehicles," *IEEE Transactions on Vehicular Technology*, vol. 69, no. 6, pp. 6053–6066, 2020.

[25] A. Masato, *Vehicle handling dynamics*, 2nd ed. Butterworth-Heinemann, 2015.

[26] G. Liu, H. Ren, S. Chen, and W. Wang, "The 3-DoF bicycle model with the simplified piecewise linear tire model," in *Proc. of the International Conference on Mechatronic Sciences, Electric Engineering and Computer (MEC)*, 2013, pp. 3530–3534.

[27] H. B. Pacejka, *Tire and vehicle dynamics*, 3rd ed. Butterworth-Heinemann, 2012.

[28] C. Chatzikomis, A. Sorniotti, P. Gruber, M. Bastin, R. Shah, and Y. Orlov, "Torque-vectoring control for an autonomous and driverless electric racing vehicle with multiple motors," *SAE International Journal of Vehicle Dynamics, Stability, and NVH*, vol. 1, 03 2017.

[29] P. Apkarian and R. J. Adams, "Advanced gain-scheduling techniques for uncertain systems," *IEEE Transactions on Control Systems Technology*, vol. 6, no. 1, pp. 21–32, 1998.

[30] W. F. Milliken and D. L. Milliken, *Race car vehicle dynamics*. UK: Society of Automotive Engineers Inc., 1996.

[31] Y. Nakajima, *Advanced tire mechanics*. Singapore: Springer Singapore, 2019.

[32] E. A. Wan and R. Van Der Merwe, "The unscented Kalman filter for nonlinear estimation," in *Proc. of the IEEE 2000 Adaptive Systems for Signal Processing, Communications, and Control Symposium*, 2000, pp. 153–158.

[33] L. R. Ray, "Nonlinear state and tire force estimation for advanced vehicle control," *IEEE Transactions on Control Systems Technology*, vol. 3, no. 1, pp. 117–124, 1995.

[34] C. V. Rao, J. B. Rawlings, and D. Q. Mayne, "Constrained state estimation for nonlinear discrete-time systems: Stability and moving horizon approximations," *IEEE Transactions on Automatic Control*, vol. 48, no. 2, pp. 246–258, 2003.